



---

## Toward Predicting Topographically Generated Turbulence

Keith W. Ayotte  
Windlab Limited, Canberra, Australia

Peter P. Sullivan and Edward G. Patton  
Meso and Micro Meteorology Division  
National Center for Atmospheric Research, Boulder, Colorado

August, 2012

## 1. INTRODUCTION - A CASE FOR A SIMPLE DIAGNOSTIC MODEL OF TOPOGRAPHIC WAKE TURBULENCE

One of the main factors driving the economics of a wind farm is the wind resource at individual turbine locations. Developers seek to maximize the wind farm yield by locating turbines in areas of highest wind, often on ridge lines in *complex* landscapes. In combination with a diligent measurement program, meso- and microscale models can be used to arrive at mean energy yields with associated uncertainty reduced to a commercially acceptable level. For assessing speedup due to topography, which is one of the main objectives in flow modelling in support of turbine placement, a Reynolds Averaged Navier Stokes (RANS) calculation can provide acceptable results in flow at the crests of hills, where turbines are most often sited. This is due mainly to two mitigating features. The first is that on the upwind side of a hill, the flow is well behaved in the sense that it is well modelled by a RANS model. The shear layer is wall bounded and the associated turbulence length scales are constrained by the proximity to the surface ( $l \sim \kappa z$ ). The second is that, to first order, the outer layer flow responds to the aggregate shape of the hill and any region of persistent separation in the lee of the hill, noting that this can be one of the significant failings of linearised models used in steep terrain. At least for thin separated regions, the aggregate hill shape and separation zone can be reasonably well represented by a RANS calculation. Therefore the RANS model is capable of creating an outer layer pressure perturbation that, to first order mimics reality, resulting in hill-top flow accelerations of sufficient accuracy to be useful in wind resource estimates. However, going hand in hand with accelerated flow over complex topographic shapes and surface types is the potential for significantly enhanced levels of turbulence in the lee of hills of even modest slope.

Our first response might be to expect a RANS formulation to perform as well as it does for simple mean flow calculations. Comparisons between RANS model output and turbulence levels in the lee of hills suggest this is not the case. Typically, RANS models of turbulence contain some physically exact components such as production and advection, but contain significant contributions from representations of second and higher moments that are less physically justified. Examples of this are the pressure-strain relation used in many second order closures such as that of Launder et al. (1975) and those that have followed from that work. The various forms of the dissipation equation used to provide a length scale in the Reynolds stress equations, or their contraction the turbulent kinetic energy equation, is also an approximation. Though a precise equation for turbulence dissipation can be derived (Stull, 1988, Pope, 2000), its solution is impractical if not impossible in the context of a RANS model. Therefore the exact form is replaced with a more tractable one that includes the familiar advection, diffusion, production and destruction formulation. The implications on the assumed turbulent characteristics of the flow can be significant. For example, in closure models of this type, the length scale of the turbulence at any point in the flow is a result of the rate of dissipation -  $\epsilon$ . Dimensionally, it follows that the length scale of the turbulence is proportional to turbulent kinetic energy ( $k$ ) to the power three-halves divided by the dissipation rate,  $\epsilon$ . This view of the turbulent length scale and associated turbulence spectrum is predicated on a single length scale that is a direct result of local mean strain in the flow. This is consistent with the theory of surface layer and mixed layer turbulence spectra of  $u_1$ ,  $u_2$  and  $u_3$  such as that presented by Kaimal and Finnigan (1994), in which energy is created within an energy containing range, transitions through the inertial sub-range and is finally dissipated in the dissipation range. For topographic wake turbulence the picture appears to be somewhat different, where for any given topographic shape it is likely that turbulent energy is created in the spectrum anisotropically at a range of scales that are in large part externally imposed by the geometry of the lower boundary and its physical characteristics. As such moving much beyond simple smooth hills with small slopes using a RANS model is difficult to justify if an accurate representation of the turbulence in the lee of a hill is sought.

In order to accurately represent the broad range of length scales present in the turbulence on the lee of a hill, eddy resolving calculations are required. In principle, predictions of the turbulence environment at any location could be obtained from metre-scale resolution Large Eddy Simulation (LES). However, even for a very modest sized wind farm, the number of grid points needed would overwhelm most of the largest institutional computational facilities in existence today, to say nothing of the typically much more modest computing resources available in a commercial environment. Predictions of when computational capabilities will increase in power and decrease in price to the point where metre-scale resolution LES calculations can be done in a commercial context are highly speculative. Similar predictions in the aircraft industry suggest decades rather than years (Spalart, 2000). In response, it is likely that solutions will be driven toward what is attainable given the current state of typical computational resources. One solution may be Detached Eddy Simulation (DES) (Spalart, 2000) or some more recently derived variation. The tradeoff for reducing the computational cost of these methods is that they become less general. In his review article Spalart (2009) points to a number of areas where DES requires application specific modification to deal with the transition from modelled to

resolved turbulence, often in wall bounded shear flows. Many of the variants of DES that follow from the original formulation are efforts to improve the performance of the original in specific situations.

A number of authors have carried out low resolution LES, Unsteady RANS (URANS) or Hybrid RANS/LES over real terrain, with varying degrees of success (see for example Silva Lopes et al., 2007, Hanjalic and Kenjeres, 2008 and Bechmann and Sorensen, 2011). The obvious advantage of this approach is that the measurements from the experiments were obtained in the real atmosphere which is ultimately what we wish to simulate. The limitation is however, the lack of systematic variation of parameters such as steepness and roughness to help understand the fundamental behaviours of such flows.

In this work we retreat back to wind tunnel observations and metre-scale resolution LES to examine and quantify the behaviour of turbulence generated in the lee of topography over a limited range of hill steepness and surface roughness. Though examined in insolation and clearly not directly representative of real terrain or situations encountered in wind farm development, examination of these cases provides some insight into the mechanisms responsible for the generation of orographic wake turbulence and how it might be quantified for use in simplified models that are more affordable in the commercial context. This report uses measurements of orographic wake turbulence measured in a boundary layer wind tunnel over a broad range of the steepness and roughness parameter space. The paper also examines results from meter-scale resolution LES of two of the wind tunnel cases, one with low slope and a relatively smooth surface where the mean flow is not separated and one with a steeper slope where the mean flow is continuously separated. We use the wind tunnel measurements and the LES to propose a scaling that helps quantify plume centre-line levels of orographic wake turbulence. We also use two-point correlation methods in LES output to examine dominant length scales in orographic wake turbulence and the coupling between inner and outer layer flow in the context of mechanisms for turbulence generation in the lee of topographic features.

This qualitative and quantitative examination of orographic wake turbulence is then used as a basis for a proposed set of diagnostic equations for orographic wake turbulence that can be used within a relatively computationally inexpensive RANS model in a commercial context. The objective is to provide a tool for identifying areas where high levels of turbulence pose a risk to wind turbines and can be further quantified using measurements.

## 2. EDDY RESOLVING CALCULATIONS OF TURBULENT WAKE FLOWS

Here we seek to gain a more clear understanding of the mechanisms involved in the generation of topographic wake turbulence and the associated length scales in the turbulence. Toward this end, two large eddy simulations were undertaken (see Section 3 for a further description of the wind tunnel cases these calculations were based on). This section describes the calculations and the results from those calculations (also see Ayotte, et al., 2010 and Sullivan et al., 2010 ).

A number of LES studies of flow over hills with and without canopies have been carried out in the recent past (e.g., Wood 2000, Brown et al. 2001, Allen and Brown 2001, Uchida and Ohya 2008, Patton and Katul 2009, and references therein). The emphasis of these studies, particularly the earlier ones, focused on understanding and predicting separation. Though turbulence production in separated topographic wakes is strong, the view taken here is broader in that we are interested in exploring wake turbulence over a wide steepness/roughness parameter space in which intermittent, persistent and no separation are present. Here two LES calculations have been undertaken, one over a hill with a shallow slope with intermittent separation and the other over a much steeper slope where the mean flow is continuous. In the context of wake turbulence production, Figure 6 shows the LES to have a similar scaling to that found in wind tunnel measurements. As such there is a high level of confidence that the LES is capturing the mechanisms responsible for wake production and therefore provides the opportunity to examine the flow in ways that are not available in wind tunnel or any other measurements. Though the number of calculations undertaken here is limited to two due to the significant expense in terms of computational time, it is expected that the main physical processes can be identified in the calculations. Work on calculations with different canonical shapes has also begun (Sullivan et al., 2010).

**Table I.** Parameters used in the LES calculations.

Case	Slope	$z_0$ (m)	$l/z_0$	Domain ( $L_x, L_y, L_z$ )(m)	Domain ( $N_x, N_y, N_z$ )
0.2S	0.2	0.08	$2.5 \times 10^3$	(3072, 1152, 1000)	(1024, 384, 256)
0.6S	0.6	0.05	$1.34 \times 10^3$	(2560, 640, 1000)	(1024, 256, 256)

## 2.1. The model

The LES code for simulating turbulent flow over terrain is based on a conventional coordinate transformation between physical and computational coordinates and adopts an incompressible Boussinesq flow model. A non-orthogonal terrain following (surface fitted) grid with a co-located arrangement of variables is employed: Cartesian velocity components  $u_1, u_2, u_3$ , pressure  $p$ , and subgrid-scale energy  $e$  are stored at cell centers with contravariant flux velocities located at cell faces. The use of flux velocities streamlines the momentum and scalar advection operators and also satisfies the (incompressible) divergence free constraint. Past work has successfully applied this methodology to time resolving turbulent simulations (both direct numerical simulations and LES) with and without thermal stratification (Sullivan et al. 2000, Sullivan and McWilliams 2002, Sullivan et al. 2008, and Patton and Katul 2009).

The LES code utilizes high-order pseudospectral differencing in horizontal coordinates and second-order finite differences in the vertical direction. A stationary iteration method is used to solve the elliptic pressure Poisson equation (Sullivan et al. 2000). The time advancement is a low-storage explicit third-order Runge-Kutta Method (Sullivan, 2004). For the present application, the lower surface is assumed to be in the fully-rough high-Reynolds-number regime, i.e. there is no resolved viscous sublayer. As is standard practice, surface momentum and scalar fluxes are then obtained by applying Monin-Obukhov similarity theory (e.g., Moeng 1984) at each surface grid point. Since the time stepping is explicit the entire algorithm, and in particular the pressure solver, is efficiently parallelized using the Message Passing Interface (MPI). The MPI domain decomposition is two-dimensional and relies on parallel matrix transposes to evaluate global operators. The entire scheme allows parallelization across a large number of processors,  $O(10^4)$  or more, and a flat-wall version of the code exhibits good strong and weak scaling (Sullivan and Patton 2008).

Two boundary-layer flows with isolated hills of varying steepness are simulated. Details of the configurations are provided in Table I. The hills are axisymmetric and sinusoidal in  $x$  with maximum steepness of (0.2, 0.6). The hill height  $H = 50$  m and thus the characteristic hill length scale  $L = (200, 67)$  m, respectively. A smoothly varying vertically stretched grid is used with spacing  $\delta z = 1$  m at the surface expanding to a maximum of 10 m at the top of the domain. The spacing in the horizontal directions is constant (i.e.,  $\delta x = \delta y$ ) with  $\delta x = (3, 2.5)$  m for the two different simulations. Large streamwise and spanwise domains are used to allow the boundary layer and hill wake to freely develop. Flow over the hill is not significantly impacted by the upper boundary since the ratio  $H/L_z = 0.05$ , where the domain height  $L_z = 1000$  m. The flows are driven by a constant pressure gradient  $1/\rho \frac{\partial p}{\partial x} = 1.63 \times 10^{-3} \text{ ms}^{-2}$  which results in winds of approximately  $10 \text{ ms}^{-1}$  at the top of the domain.

In order to minimize the computational effort, each simulation was started from random initial perturbations with the hill absent, i.e. simulating turbulence over a flat lower boundary. After approximately 10 large eddy turnover times (about 100,000 time steps), fully developed turbulent boundary layers fill the computational domain. At this point the LES was restarted inserting the hill at the center of the domain. We note that Gong et al. (1996) adopted a similar strategy in their approach to simulating turbulent flow over sinusoidal bumps in a wind tunnel. This strategy is advantageous since the wake turbulence downstream from the hill is not continually recycled into the upstream domain so that the resulting flow is more representative of a wind tunnel boundary-layer flow over an isolated hill. This technique allows us to average over an ensemble of realizations where each realization is started from a different flat volume. These simulations are carried out utilizing 4096 processors on a Cray XT4. Each processor operates on about 16,384 grid points, which is near the minimal amount for adequate overall performance. With the hill in place, the computational effort is dominated by the solution of the pressure Poisson equation, approximately 50% of the total time. 2-D planes and 3-D volumes of turbulence data are archived after the hill is inserted into the flow and are used for flow visualization and computation of statistics.

Figure 1 shows measured (a) and modelled (b) cross-sections of  $\overline{u'_1 u'_1}$ , normalised by  $u_*^2$  from the upstream flow. The figure shows similar behaviour with respect to the location of the source region and the downwind extension of the turbulent plume once generated in the lee of the hill. The normalised plume centerline values are compared in Figure 11.

## 2.2. Wake turbulence generation

Figures 2 and 3 show instantaneous view of the LES flows for the 0.2S and 0.6S cases respectively.\* Though quite different in character, the realizations have marked similarities in the flow upstream of the hill crest. Specifically the flow is strongly sheared near the surface with a thin shear layer projecting into the lee of the

---

\* Both figures have a vertical exaggeration of 3.

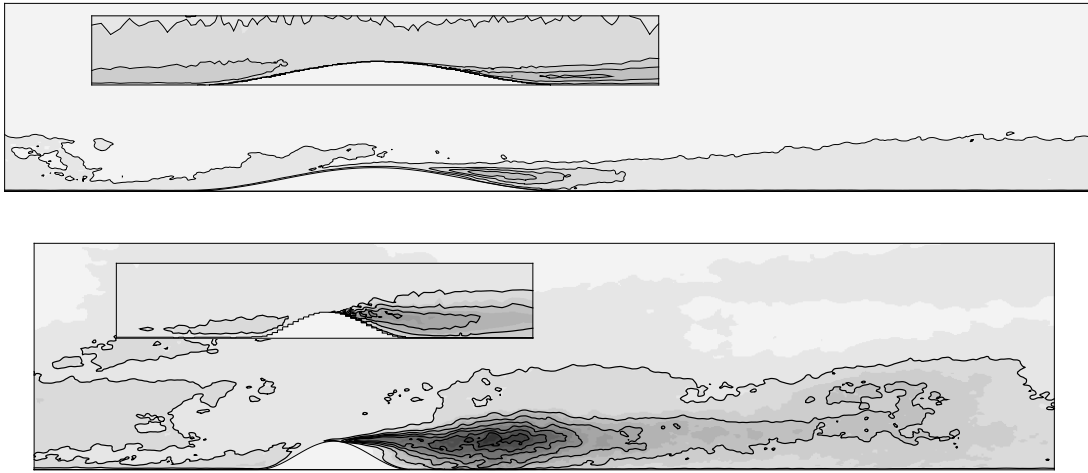


**Figure 1.** LES and Measured (inset) cross-sections or streamwise normal stress normalized by  $u_*^2$  for 0.2S (upper) and 0.6S (lower) cases. Contour interval is 5 for the 0.2S case and 10 for the 0.6S case.

hill crest. Both flows then become quite turbulent with eddies containing length scales ranging from that of ground based shear to  $L$ , the half-length of the respective hills. For the 0.2S case, the flow stays somewhat coherent for some distance downwind from the hill crest. Moving images of the flow show that distance varying through time, intermittently moving further downstream to almost the leeward base of the hill with eddies intermittently shearing away from the surface as the momentarily coherent flow breaks into turbulent motion. This is in striking contrast to the 0.6S case where the surface based coherent stream separates immediately in the lee of the hill crest, meandering rapidly and quickly breaking into vigorous turbulent motions. This is consistent with the view of the production mechanism that will be presented in the next section.

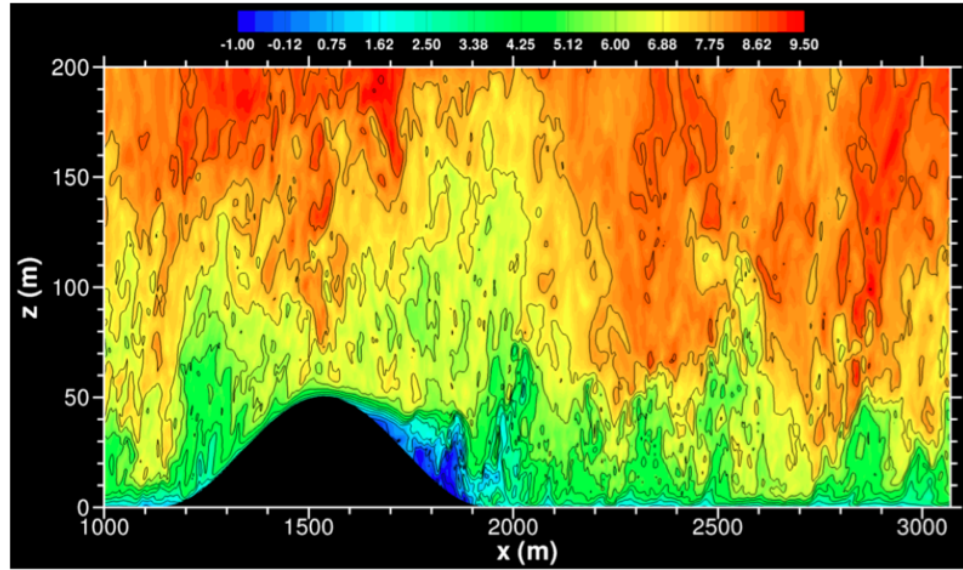


**Figure 2.** Instantaneous vertical cross-section of  $U_1$  for 0.2S LES case. Scale at top of image is in units of  $\text{ms}^{-1}$ .

### 2.3. Length scales in topographic wake flows

The complex spatial structure of a hill wake and its dependence on hill slope and roughness are shown in Figures 2 and 3. We also note above that there is a significant increase in turbulence length scale in the lee of

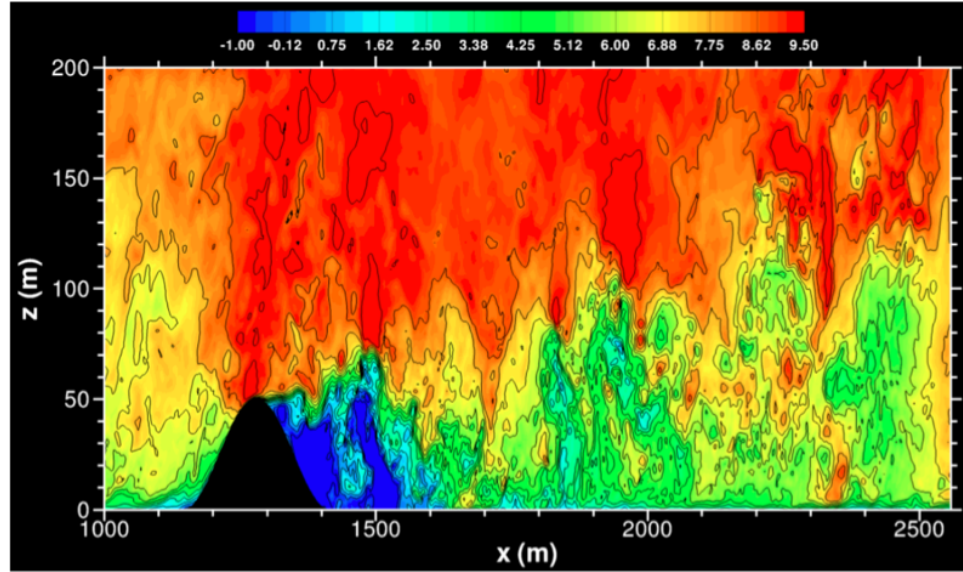


**Figure 3.** Instantaneous vertical cross-section of  $U_1$  for 0.6S LES case. Scale at top of image is in units of  $\text{ms}^{-1}$ .

a hill as the flow moves into the mean adverse pressure gradient created by the hill. From the LES database, we can calculate the two-point spatial correlations:

$$R_{uu}(x, z) = \frac{\langle u(x, z)u(x_{ref}, z_{ref}) \rangle_{yt}}{\sqrt{\langle u^2(x, z) \rangle_{yt}}\sqrt{\langle u^2(x_{ref}, z_{ref}) \rangle_{yt}}} \quad (1)$$

where  $(x_{ref}, z_{ref})$  denotes a reference point and  $u(x, z)$  is the velocity perturbation from the  $y$ - and time-averaged mean (Dupont et al. 2008). Statistics are obtained by averaging over the final five output volumes from the LES calculation, a period of about 60 seconds. Here, we use  $R_{uu}(x, z)$  in a number of ways: 1) to indicate turbulence length scales in different flow regions, i.e. to shed light on length scale changes as the flow moves past the hill, and 2) to look for evidence of coupling between near surface flow and perturbations originating in the outer layer.

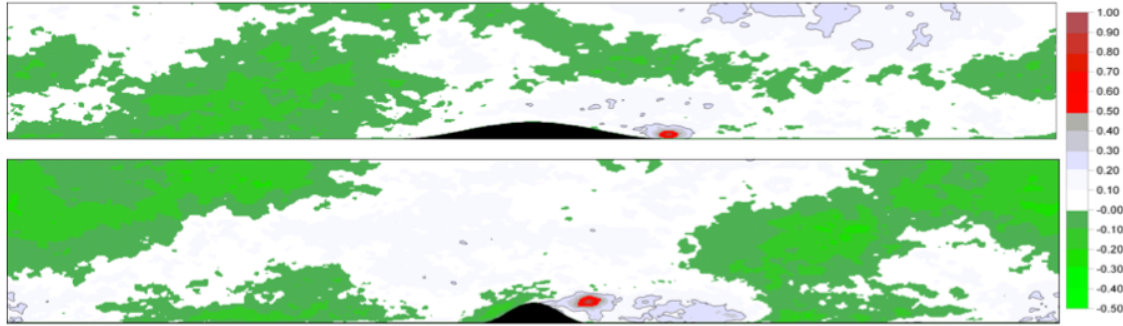


**Figure 4.** Two-point correlation coefficient  $R_{uu}$  at  $x = 2L$  at the plume centreline. Scale appears at the right of the figure with red indicating positive correlation and green indicating negative correlation.

The cross sections in Figure 4 show  $R_{uu}$  with a reference point near the plume centerline at the downwind end of the hill ( $x = 2L$ ). In these cross sections, the colour scale ranges from -0.5 (green) to 1.0 (red). The higher correlations and their larger spatial extent are indicative of an increased eddy length scale. It is interesting to note that for the 0.6 slope case (lower image in Figure 4), the area of strong correlation is limited to a compact area around the reference point, which is consistent with the depth of the wake plume in Figure 1. The region of strong correlation for the 0.2 slope case is approximately the same size, extends

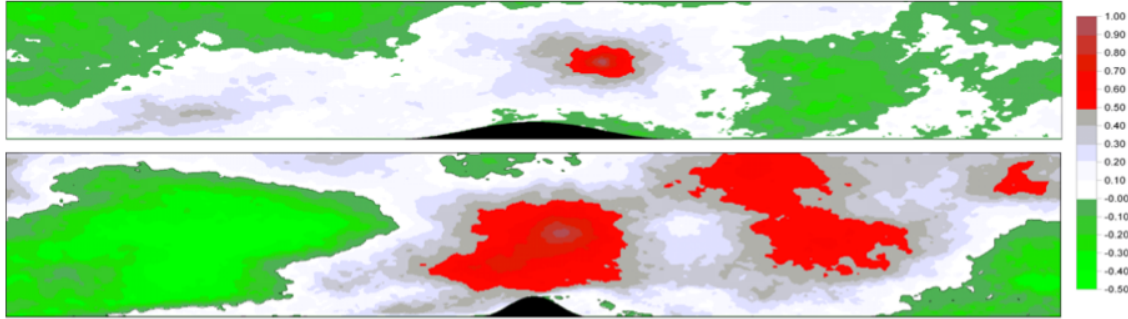


**Figure 5.** Two-point correlation coefficient  $R_{uu}$  at  $x = 2L$  and  $z = 200\text{m}$ , well into the outer layer flow. Scale appears at the right of the figure with red indicating positive correlation and green indicating negative correlation.

beyond the full height of the hill, and has a similar horizontal extent to that of the 0.6 slope case. This indicates that the length scales associated with the turbulence created further down the slope are of a similar size to those in the 0.6 slope case. The two cross sections in Figure 5 show  $R_{uu}$  calculated at  $(x_{ref}, z_{ref}) = (L, 200\text{ m})$ , i.e. well into the outer layer of the flow. In this figure, the colour scale is as in Figure 4. In the 0.6 slope case, there is almost no negative correlation near the downwind face of the hill, whereas for the 0.2 slope case there is a region of significant negative correlation, suggesting a coupling between the outer layer flow and the near surface flow in the region of strongest wake turbulence production. The reason for this appears to be that for the low slope case, the adverse pressure gradient created in the lee of the hill is of comparable magnitude to the fluctuating pressure gradients projected down to the surface from the outer layer flow. As such the turbulence has a component that is coupled with the turbulence originating in the outer layer and also therefore shares some of the length scales of that outer layer turbulence. Alternatively, for the steep case where the adverse pressure gradient is strong relative to the pressure perturbations originating to the outer layer, there is very little coupling between the turbulence in the outer layer flow and the wake turbulence as the mean pressure perturbation from the hill dominates the flow and turbulence generation.

### 3. WAKES IN THE LEE OF TOPOGRAPHIC FEATURES BASED ON WIND TUNNEL MEASUREMENTS

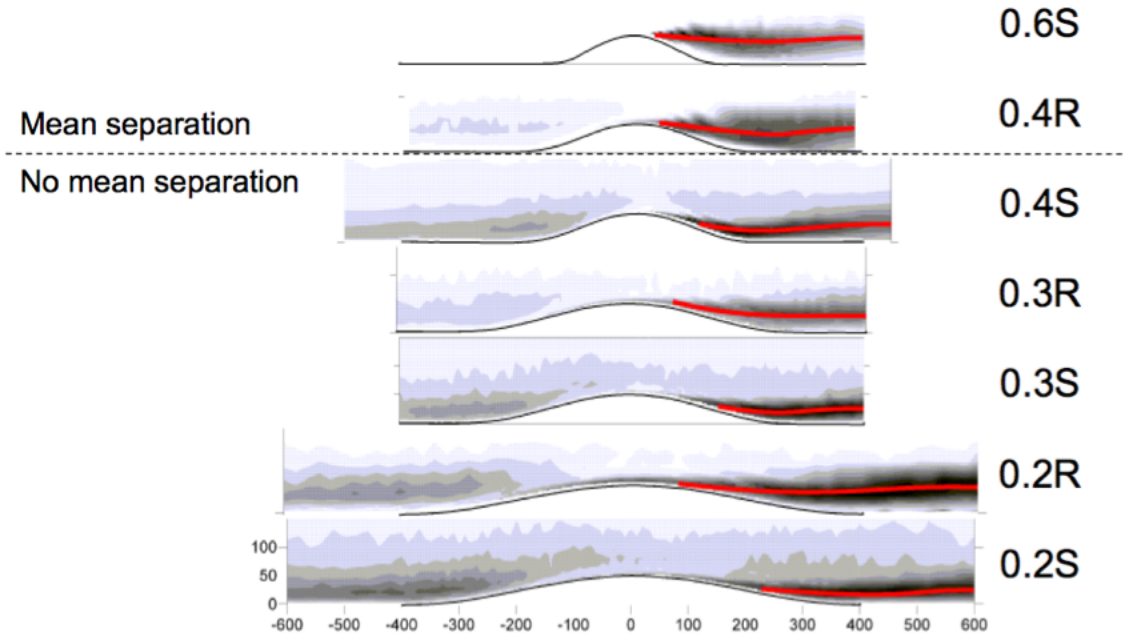
Ayotte and Hughes (2004) present measurements from wind tunnel flows over axi-symmetric, sinusoidal hills of varying steepness and roughness. The aim of that study is to clarify the behaviour of mean flow and turbulence in flows spanning a parameter space that: 1) includes small perturbations for which simple linear flow models are expected to give reasonably accurate solutions, and 2) fully separated flow in which nonlinear effects dominate. Table II lists the parameters for each of the wind tunnel runs.

Figure 6 shows vertical cross sections of measurements of streamwise normal Reynolds stress,  $\overline{u'_1 u'_1}$ , where  $u'_1$  is the perturbation from the time averaged streamwise component of the velocity. The cross sections are labeled by their maximum slope (0.2–0.6) and surface roughness (S, R). The hills are of the same height (50 mm) with varying hill half lengths ( $L$ , see Figure 7) which gives a range of steepness and  $L/z_0$  values ranging from  $2.5 \times 10^2$  to  $3.0 \times 10^3$ . See Ayotte and Hughes (2004) for a more complete description of the experiment. In the figure the darker shades represent higher levels of  $u'_1 u'_1$  with the shading/contour scale varying between cases.

In Figure 6 we can see the consistent plume-like structure of the wake turbulence and a pronounced difference in the source location of the turbulence relative to the hill. The red lines in the figures are the plume centrelines. For similar slopes, the source region moves from the base of the hill for smooth surfaces (0.2S) toward the hill crest for the rougher surface (0.2R). Similarly, the source region moves toward the crest of the hill with increasing hill slope. For the two strongly separated cases (0.4R and 0.6S), the source region is at or very near the hill crest and extends downwind above the region of reversed mean flow. Plume-like behaviour similar to that in the 0.6S case has been well documented in the literature by, for example, Uchida

**Table II.** Hill and flow parameters. Run designations ending in R and S are rough and smooth respectively. Values of  $z_0$  are taken from fully adjusted flow immediately upstream from hill.

Run	Slope	$z_0$ (mm)	$u_*$ ( $\text{ms}^{-1}$ )	$L$ (mm)	$L/z_0$	$l_i$ (mm)	$l_i/z_0$	$h_m$ (mm)
0.2S	0.2	0.08	0.524	200	2500	12.6	158	76.4
0.2R	0.2	0.80	0.720	200	250	19.9	24.9	91.8
0.3S	0.3	0.04	0.493	140	3500	8.4	210	52.3
0.3R	0.3	0.40	0.637	140	350	12.9	32.3	62.3
0.4S	0.4	0.03	0.486	100	3330	6.0	200	37.5
0.4R	0.4	0.40	0.641	100	250	10.0	25.0	45.9
0.6S	0.6	0.05	0.510	67	1340	4.7	94.0	26.7



**Figure 6.** Vertical cross-sections of streamwise normal stress normalised by shear stress  $\overline{u'_1 u'_1} / u_*^2$  from wind tunnel measurements. Dashed lines are plume centrelines. Contour intervals are 1.0, 2.0, 3.0 and 5.0 for the 0.2, 0.3, 0.4 and 0.6 slope cases respectively. 0.4R and 0.6S cases have persistent separation in the lee of the hill.

and Ohya, (2008). However, this variation in plume behaviour over the range of surface roughness and slope has not been well documented.

### 3.1. A simple scaling for topographic wake turbulence

In order to understand the physical mechanism for turbulence production and transport in a quantitative way we need to compare the behaviour of the turbulence over the steepness and roughness parameter space of the wind tunnel experiment. To do this, we begin by recalling the linear theory of flow over low hills. Using the linear theory of Jackson and Hunt (1975), the flow over a hill can be divided vertically into a number of regions (Hunt et al., 1988). The layer of the flow near the surface is referred to as the inner layer (see Figure 2). The maximum mean flow speedup occurs within the inner layer ( $z = l_m$ ) at a height of one-third to one-half of the inner layer depth. By definition, at the top of this layer the advection time scale  $T_A$  is similar to the Lagrangian time scale  $T_L$ . The top of the inner layer is at  $z = l_i$  where  $l_i \ln(l_i) = 2\kappa^2 L$  and  $\kappa$  is von Karmans constant (Belcher and Hunt, 1998). In the lower portion of the inner layer,  $T_L \ll T_A$  suggesting that turbulence is in local equilibrium with dissipation, matching production. In their Figure 2, Belcher and Hunt (1998) show for hills of low slope that production closely matches dissipation integrated along streamlines up to the hill crest. However over steeper hills, as the flow encounters the adverse pressure gradient on the downwind side of the hill, turbulent length scales rapidly change from being constrained by proximity to the

surface (varying like  $\kappa z$  for  $z < l_i$ ) to length scales associated with the elevated shear layer (or as we show later, by pressure perturbations imposed by turbulence in the outer layer). In any case, the length scales in the lee of the hill are much greater than those in the flow upstream of the hill crest, which has the effect of significantly reducing dissipation in the lee of the hill, creating an imbalance such that production is much greater than dissipation directly in the lee of the hill crest.

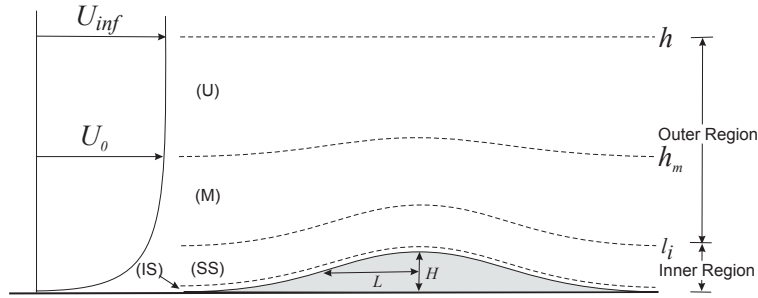


**Figure 7.** Flow over a shallow hill divided into layers after Hunt et al. (1981).

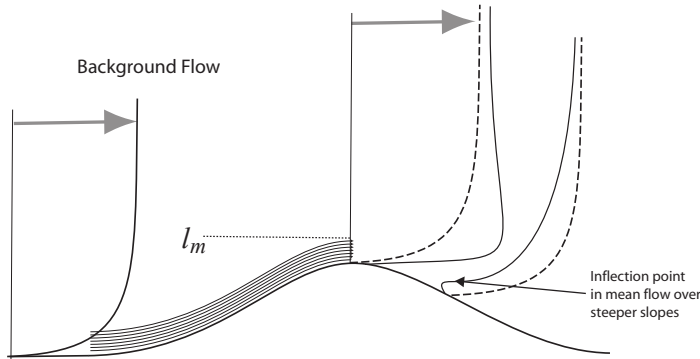


**Figure 8.** Hill crest and leeward profiles of accelerated flow over a hill. Dashed lines in hill crest and leeward profiles are upstream flow.

On the upwind side of a simple hill, the linear theory of flow over a hill holds reasonably well. On the leeward side of the hill crest, as the flow enters a region of adverse pressure gradient, a strong departure from linear theory occurs. The mean flow decelerates and may detach from the hill face and reverse either intermittently or continuously, depending upon the strength of the adverse pressure gradient which is in turn a result of the hill slope. This process will be demonstrated later using LES results. In examining the mechanism for turbulence generation in the lee of the hill more closely, Figure 3 shows accelerated mean flow profiles over an axi-symmetric sinusoidal hill. The accelerated flow has a maximum at the hill crest and then decelerates in the adverse pressure gradient on the lee side of the hill as noted above. This is an area of rapid turbulence growth. For steeper slopes with a strong adverse pressure gradient, an associated inflection point in the mean profile may form in the decelerated flow. The strength of this inflection point, if present, and the distance downstream from the hill crest where the inflection point forms is dependent upon the strength of the adverse pressure gradient that in turn scales with the hill slope. Stability theory (Drazin, 2002) shows that Rayleigh instabilities near the inflection point in the mean profile in the lee of the hill will grow rapidly and ultimately break into turbulent motions, transforming momentum in the mean flow into turbulent motions that are then advected downstream. The fact that turbulence forms in the lee of less steep hills without inflected mean profiles implies that an inflection in the mean profile and its associated dynamic instability is clearly not the only trigger or indicator for rapid turbulence growth. However, for steep slopes it is likely to play a leading role. Here we will simply refer to a region of rapid turbulence growth. Hill length and surface roughness also

play a role in that they determine the height of the maximum speedup ( $l_m$ ) and the amount of momentum an average parcel has as it enters the region of adverse pressure gradient and therefore its propensity to reverse direction in the adverse pressure gradient. As the flow traverses the hill into the area of adverse pressure gradient, it undergoes a characteristic transition from relatively smooth flow containing small scale eddies ( $l < \kappa z$ ) to strongly turbulent flow containing much larger eddies that have length scales characteristic of the mean shear (surface based or elevated above a region of separation), the length and height of the hill and in some cases over shallow hills with weak adverse pressure gradients, length scales imposed from the outer layer flow. Figures 9 and 10 show this mechanism for hills of moderate and large slope respectively. In the former a region of rapid turbulence growth develops some distance downstream of the crest and the turbulence growth is somewhat weaker. For the steeper slope with mean separation, the situation gives rise to strong shear at the top of the mean region of recirculation an associated inflection point is also created. The strong shear and inflection point instability give rise to a turbulent plume forming nearly immediately downstream of the hill crest. This will be shown more clearly and quantitatively in the LES results presented later.

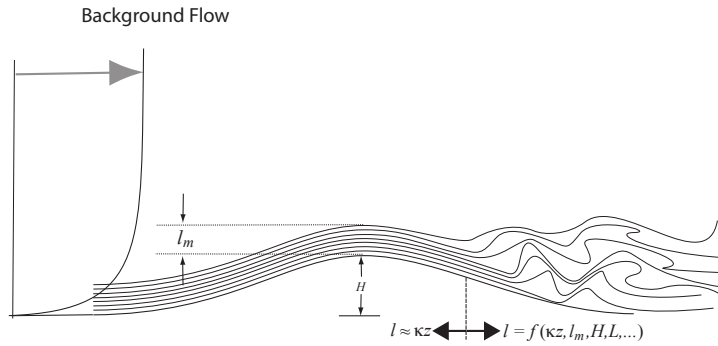


**Figure 9.** Flow becoming turbulent over a shallow hill.

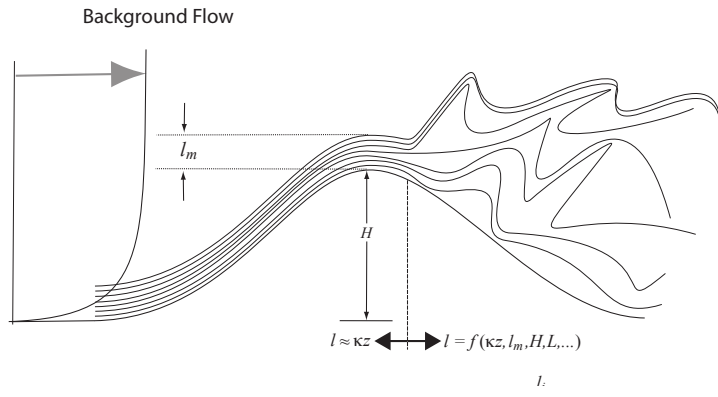


**Figure 10.** Flow becoming turbulent over a steep hill.

As noted above, at the hill crest, below the maximum speedup ( $z < l_m$ ), turbulence is in local equilibrium, with production and dissipation approximately matched in the strong, surface based mean strain. In this region the turbulent length scales are of order  $\kappa z$ . However, as the flow moves past the hill crest into the area of adverse pressure gradient, the strong shear stress and mean strain near the surface in the accelerated mean flow feed the region of instability and rapid turbulence growth in the lee of the hill. This enhanced mean strain and shear stress can be viewed as topographic wake turbulence production potential and can be used to quantify the expected levels of wake turbulence in the lee of the hill crest. In this simple picture of wake turbulence production, the limiting factors are the upstream shear stress and the mean strain at the hill crest. Integrating this production potential from the surface up to the level of maximum speedup ( $l_m$ ), we can arrive at a value for the production potential that contains the shear stress ( $u_*^2$ ), the surface roughness

parameter ( $z_0$ ) and  $l_m$  and can be used to normalize the plume centerline values of the streamwise normal stress at the downwind base of the hill. To see this, we begin with the production of  $\overline{u'_1 u'_1}$ ,

$$P_{11} = - \left\{ \overline{u'_1 u'_1} \frac{\partial U_1}{\partial x_1} + \overline{u'_1 u'_2} \frac{\partial U_1}{\partial x_2} + \overline{u'_1 u'_3} \frac{\partial U_1}{\partial x_3} \right\} \approx u_*^2 \frac{\partial U_1}{\partial x_3} \quad (2)$$

Integrating the shear from the surface to the height of maximum speedup,

$$\int_0^{l_m} \frac{\partial U_1}{\partial x_3} dx_3 = U_1(l_m) \propto \ln \left( \frac{l_m}{z_0} \right) \quad (3)$$

yields an expression for the production potential that can be used to normalise the plume centerline values of  $\overline{u'_1 u'_1}$ ,

$$P_{11} \propto u_*^2 \ln \left( \frac{l_m}{z_0} \right) \quad (4)$$

Figure 11 shows plume centerline values of  $\overline{u'_1 u'_1}$  at  $x = 2L$  normalised by the production potential ( $u_*^2 \ln(l_m/z_0)$ ). The open symbols are the wind tunnel measurements for the smooth (diamond) and rough (square) cases while the filled triangles are from the LES results. When normalised by the production potential, the linearity of the relationship suggests that plume centerline values of  $\overline{u'_1 u'_1}$  are determined by the rate at which the region of instability is fed by the production potential and the adverse pressure gradient that in turn scales with hill slope.

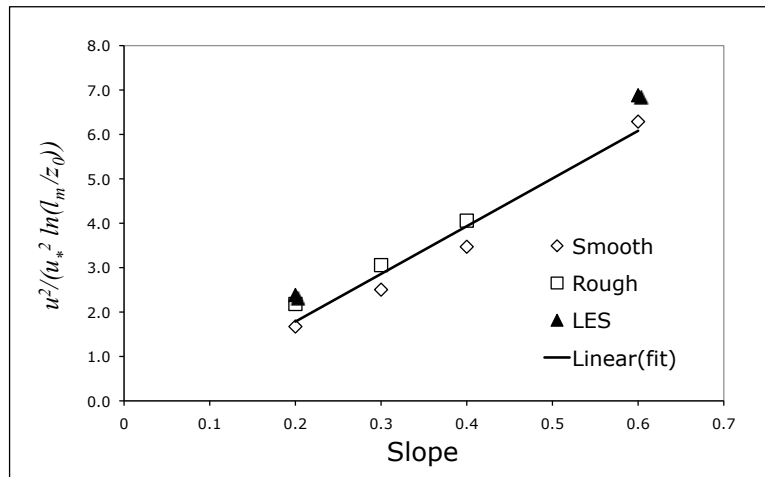


**Figure 11.** Normalised centreline values of streamwise normal stress,  $\overline{u'_1 u'_1}$ , at  $x = 2L$ . Open symbols are wind tunnel measurements, closed triangles are LES

#### 4. CONCLUDING REMARKS

Linear theory of flow over hills has been used to describe turbulent flow on the windward side of a hill before it responds to an adverse pressure gradient past the crest of a hill. This has allowed us to characterise the flow in terms of its potential to produce orographic wake turbulence. A scaling is presented in which levels of plume centre-line turbulence can be predicted for simple hill shapes under neutral stratification. Flow approaching an isolated hill is wall bounded shear flow. The turbulence length scales in the near surface flow are constrained by the proximity to the surface and vary like  $\kappa z$ . Any number of turbulence closures used in RANS modelling ranging from single equation mixing length models to complex second order closures employing equations for all of the second moments and a dissipation equation, are capable of modelling such flows. In fact many of these models were created specifically for and calibrated using wall bounded shear flows. Where models of this type begin to break down is where externally imposed length scales begin to become important in the flow and the simple length scale specification is not up to the task. The transition between these two states occurs as the flow encounters the adverse pressure gradient in the lee of the hill crest

after being strongly sheared as it accelerates up the windward slope. In this region of strong mean shear and adverse pressure gradient, conditions are favourable for small perturbations to grow rapidly, extracting energy from larger scale motions. Rapidly growing turbulent motions in this region, though initially having length scales associated with the local shear in the mean profile, evolve rapidly to have length scales determined by the strength and horizontal and vertical length scales of the region of adverse pressure gradient.

Though perhaps somewhat idealised, the picture presented in this work is one where a region of instability and rapid turbulence growth forms in the lee of the hill crest. The conditions conducive to rapid turbulence growth in this region are stronger and form more quickly (closer to the hill crest) for steeper hills. Conversely for lower hills, these conditions form more slowly and the region of instability reaches its maximum somewhat further down the lee slope. Here this process is described as a region of instability being fed by turbulent, strongly sheared flow. In this characterisation, the strength of the mean shear at the hill crest and the strength of the adverse pressure gradient in the lee of the hill are the main controls on the growth of turbulence in the lee of the hill. The former is well modelled using a RANS turbulence closure. The latter is imposed from the flow in the middle and outer layers (Belcher and Hunt, 1998) and is driven by the shape and the horizontal and vertical length scales of the topographic perturbation. These length scales are externally imposed on the flow as boundary conditions and are not well represented in a RANS closure that models production and dissipation based on local rates of mean strain.

#### 4.1. Toward wind farm scale eddy resolving calculations

The physical processes described and partially quantified here, suggest that single-point RANS turbulence closures, at least as currently formulated, are unlikely to be able to represent the externally forced length scales associated with the rapid growth of turbulent motions in the lee of wind farm scale topographic features. This raises the question of how such calculations can be done so that they accurately capture the rapid growth of turbulent motions and their subsequent advection downstream, where they may impinge on wind turbines or other structures in their path.

Sullivan et al. (2010) present Large Eddy Simulations (LES) of an atmospheric planetary boundary layer (PBL) on a curvilinear grid over a number of prototypical shapes to examine the interaction of turbulent PBL flow with landscape features. This study contains calculations at resolutions of 2.5m in the x- and y-directions and 1m in the vertical direction at the surface. Though valuable in the scientific context, calculations of this nature are currently unreachable in a commercial context over the real terrain of a wind farm. Though still quite expensive and technically difficult to carry out, a number of authors have carried out low resolution LES, Unsteady RANS (URANS) or Hybrid RANS/LES over real terrain, with varying degrees of success (see for example Silva Lopes et al., 2007, Hanjalic and Kenjeres, 2008 and Bechmann and Sorensen, 2011). However, even for a very modest sized wind farm, the number of grid points needed for a well resolved LES would overwhelm most of the largest institutional computational facilities in existence today, to say nothing of the typically much more modest computing resources available in a commercial environment.

Predictions of when computational capabilities will increase in power and decrease in price to the point where metre scale resolution LES calculations can be done in a commercial context, are highly speculative. Similar predictions in the aircraft industry suggest decades rather than years (Spalart, 2000). In response, it is likely that solutions will be driven toward what is attainable given the current state of typical computational resources. One solution may be Detached Eddy Simulation (DES) (Spalart, 2000) or some more recently derived variation. The tradeoff for reducing the computational cost of these methods is that they become less general. In his review article on DES, Spalart (2009) states "*Separation is the essential flow feature motivating DES, with the expectation that the boundary layer is treated with RANS and is quasi-steady, but the free shear layer it feeds develops LES content.*" By this description, at least for simple hill shapes like the ones examined in this work, DES or some variant thereof, appears to be a close match for the physics present in these flows. The wall bounded shear flow upstream of the hill crest is well suited to RANS treatment while in the lee of the hill the flow transitions to a persistent or intermittent elevated free shear flow. The analysis of the flow presented herein suggests that DES may be a viable option for commercial eddy resolving calculations.

## REFERENCES

1. Ayotte, K.W. and Hughes, D.E., 2004, Observations of boundary-layer wind-tunnel flow over isolated ridges of varying steepness and roughness, *Boundary-Layer Meteorol.*, **112**, 525-556
2. Bechmann, A. and Sorensen, N.N., 2011, Hybrid RANS/LES applied to complex terrain, *Wind Energy*, **14**, 225-237

3. Belcher, S.E. and Hunt, J.C.R., 1998, Turbulent flow over hills and waves, *Annu. Rev. Fluid Mech.*, **30**, 507-538
4. Drazin, P. G., 2002, *Introduction to hydrodynamic stability*, Cambridge University Press, Cambridge Texts in Applied Mathematics, Cambridge, England.
5. Hunt, J.C.R., Leibovich, S. and Richards, K.J., 1998, Turbulent shear flow over low hills, *Quart. J. Roy. Meteorol. Soc.*, **114**, 1435-1471
6. Hanjalic, K. and Kenjeres, S., 2008, Some developments in turbulence modeling for wind and environmental engineering, *Journal of Wind Engineering and Industrial Aerodynamics*, **96**, 1537-1570.
7. Kaimal, J.C. and J.J. Finnigan, 1994, *Atmospheric Boundary Layer Flows*, Oxford Univ. Press, New York.
8. Jackson, P.S. and Hunt, J.C.R., 1975, Turbulent flow over a low hill, *Quart. J. Roy. Meteorol. Soc.*, **101**, 929-955
9. Launder, B.E., Reece, G.T. and Rodi, W., 1975, The development of a Reynolds Stress Turbulence Closure, *J. Fluid Mech.*, **68**, 537-566
10. Pope, S.B., 2000, *Turbulent Flows*, Cambridge University Press, Cambridge, UK, 771pp
11. Silva Lopes, A., Palma, J.M.L.M. and Castro, F.A., 2007, *Boundary-Layer Meteorol.*, **125**, 85-108
12. Spalart, P., 2000, Strategies for turbulence modelling and simulations, *Int. J. Heat and Fluid Flow*, **21**, 252-263
13. Spalart, P.R., 2009, Detached-Eddy Simulation, *Annu. Rev. Fluid Mech.*, **41**, 181-2002
14. Stull, R.B, 1998, *An Introduction to Boundary Layer Meteorology*, Kluwer Academic Press, 666p
15. Sullivan, P.P., Patton, EG, and Ayotte, K.W., 2010: *Turbulent flow over and around sinusoidal bumps, hills, gaps and craters derived from large eddy simulations.*, 19th Conference on Boundary Layer and Turbulence , Keystone, CO.
16. Uchida, U. and Ohya, Y, 2008, Micro-siting technique for wind turbine generators by using large-eddy simulation, *Journal of Wind Engineering and Industrial Aerodynamics*, **96**, 2121-2138